



Influence of corrosion on the ultimate compressive strength of steel plates and stiffened panels



S. Sultana^a, Y. Wang^{a,b,*}, A.J. Sobey^a, J.A. Wharton^b, R.A. Shenoi^a

^a Southampton Marine and Maritime Institute, University of Southampton, Boldrewood Innovation Campus, Southampton SO16 7QF, UK

^b National Centre of Advanced Tribology at Southampton (nCATS), Engineering and the Environment, University of Southampton, Highfield Campus, Southampton SO17 1BJ, UK

ARTICLE INFO

Article history:

Received 21 May 2015

Received in revised form

6 August 2015

Accepted 6 August 2015

Keywords:

Nonlinear finite element analysis

Ultimate strength

Pitting corrosion

Steel plate

Stiffened panel

ABSTRACT

This study concentrates on a comparison between steel plate and stiffened panels subject to localised corrosion. A finite element analysis is used to investigate the effect of random corrosion on the compressive strength capacity of marine structural units. Variables include the extent of corrosion; slenderness ratio and aspect ratio. A corrosion prediction model is incorporated to determine the thickness reduction with time. Corrosion-induced volume loss results in a greater reduction of ultimate strength for slender plates compared to stiffened panels, up to 45%, showing the structural element selection can strongly influence the accuracy of the estimated corrosion damage effect.

© 2015 Elsevier Ltd. All rights reserved.

1. Introduction

Corrosion is a problem for a large number of steel structures. The ability to model this corrosion is vital to understand the behaviour of a structure through its life, rather than just after deployment. Corrosion damage is especially prevalent in marine structures due to the constant exposure to the harsh environment and to the highly corrosive cargo transported by ships such as crude oil, iron ore and coal. Empirical evidence shows that corrosion is one of the main five damage causes which lead to loss of ships [1]. Corrosion mechanisms lead to thinning of the structural material, a change in its mechanical properties and ultimately a decrease in its strength capacity [2]. Major oil spill accidents such as the Erika (1999), Castor (2000) and Prestige (2002) [3] have highlighted the importance of the corrosion assessment on the strength of structures.

A review on corrosion predictions in the marine environment and the corrosion effects on the structural strength capacity can be found in Wang et al. [4]. Various corrosion prediction models have been proposed in the literature, including mathematical models based on mechanistic principles [5] and statistical models based on actual corrosion data [6–9], where Ref. [6] analysed the statistical scatter of corrosion damage using a Weibull function at any

time point and which has been proven to work well by further studies [7,8], even for subsea environments. When comparing these approaches Jiang and Guedes Soares [10] propose that statistical models based on data from different ages and locations is more versatile and can be used to analyse a wide range of marine structures. A number of nonlinear finite element analysis (FEA) has been carried out to investigate the influence of these models on the strength capacity of structures. Saad-Eldeen et al. [11] modelled a box girder, representing the large structural scale, and this showed that corrosion can affect the compartment level ultimate strength but, due to the computational time, often makes systematic studies difficult. Studies at the smaller structural scale [12–17] allow for a large quantity of data to be analysed. However, despite the ever improving modelling techniques, there are still challenging issues including the realisation of one-side localised corrosion using shell elements, rough surface on the corroded area and cracking associated with pits. In addition, small scaled models with detailed corrosion features may not accurately reflect the global behaviour of a corroded structure. The transmission of the corrosion effect from large to small scale has yet to be fully understood. The present work explores the comparison between plate and larger structural units. Following on from the authors' previous work [16], which focused on the corrosion location and microbial attack on plate elements, this study investigates the effects of a number of geometrical parameters and considers a newly developed stiffened panel model. This allows the examination of the ultimate strength of different structural configurations and provides insights in the structural element selection when

* Corresponding author at: Southampton Marine and Maritime Institute, University of Southampton, Boldrewood Innovation Campus, Southampton SO16 7QF, UK. Fax: +44 2380593016.

E-mail address: yw4u14@soton.ac.uk (Y. Wang).

assessing the corrosion influence. Based on a review of the literature [6–10], a statistical corrosion prediction model is used to inform the temporal damage extent for different locations in a ship hull.

2. Modelling structures subjected to pitting corrosion

2.1. Ultimate strength modelling

Structural failure is normally associated with material and geometric nonlinearities. The former is related to yielding or plastic deformation, whilst the latter is due to buckling or large deflections [18]. To incorporate such features, structural strength assessment is undertaken through a nonlinear FEA procedure in ANSYS 14.5. An elastic perfectly plastic material model is used for the material nonlinear properties. For all the models, the large deflection static analysis is used to achieve the geometric nonlinearities, with full Newton–Raphson method and automatic time stepping. The structural models are generated using a shell element SHELL181 (a 4-node element representing the mid-plane of a structure), which is typically used for thin-walled structures [4]. The resulting stress and deflection values for each corrosion case are then analysed to understand how the structure responds to a range of parameters.

2.2. Application of corrosion model

Based on the corrosion data collected from different locations in bulk carriers [19], the present study makes use of the nonlinear time-dependant corrosion model proposed by Qin and Cui [9] to predict the depth of the random corrosion pitting after a number of years in service, see Eq. (1)

$$d(t) = d_{\infty} \left\{ 1 - \exp \left[- \left(\left(\frac{t - T_{st}}{\eta} \right)^{\beta} \right) \right] \right\}, \quad (1)$$

where $d(t)$ is the thickness reduction due to corrosion, mm, at various time point t , y ; d_{∞} is the long-term corrosion wastage, mm; T_{st} is the pitting corrosion initiation time point, y and β and η are parameters determined by collected data. In the present research the corrosion data for different plate locations of bulk carriers gathered by Paik et al. are used to deduce d_{∞} , T_{st} , β and η . One of the benefits of this model is that it takes into consideration the time when pitting corrosion initiates unlike most existing models.

Moreover, parameters can be quickly determined based on the survey data compared to the first principle model proposed by Melchers et al. [5].

Paik et al. [19] gathered a total of 7503 thickness measurements from 16 different structural locations on 44 bulk carriers (up to 20 years in service). Six structural locations are studied here, including bottom plates (BP), inner bottom plates (IBP), lower slopping plates (LSP), lower wing tank side shells (LWTSS), side shells (SS) and upper wing tank side shells (UWTSS). A schematic of the location of these plate components is represented in Fig. 1 [19]. Using the least-square method, the long term corrosion wastage thickness d_{∞} is assumed to be different for different locations. The value of the time at which corrosion initiates T_{st} is assumed to be equivalent to 7 years for all cases. Due to the high uncertainties in the corrosion database, all parameters are assumed to be random rather than deterministic. The Qin and Cui [9] model may not be representative of all marine corrosion conditions and the characteristics of corrosion may differ with environment and operating conditions. However, this study does not intend to investigate the adaptability of such corrosion prediction models, and those available in the literature can be used for other conditions.

The results of the corrosion model application together with the measured data are shown in Fig. 2, which shows that the behaviour of the model varies depending on the structural location. The BP and LWTSS thickness reductions follow a nearly linear trend, while nonlinear changes were obtained for the other locations. However, the highly scattered data points are probably due to the data collected from the renewed plates at around 15 years old.

2.3. Model construction

The results shown in Fig. 2 are used to determine the thickness reduction for the simulated structural members. Circular shaped pits are distributed randomly on the structural surface with the degree of pitting (DOP, percentage of pitted area to the entire surface area) ranging between 10, 20 and 30%. Fig. 3 shows plate models for each DOP with simply supported boundary condition. The simulated corrosion pattern is similar to that observed during ship surveys [20]. The upper limit of DOP is based on the current classification regulations on the allowable wastage [21]. The lower limit is chosen to align with Daidola et al.'s findings [22], who reported that pitting corrosion only becomes effective when the intensity is above 10–20%. The pit depths for 10, 15, 20 and 25

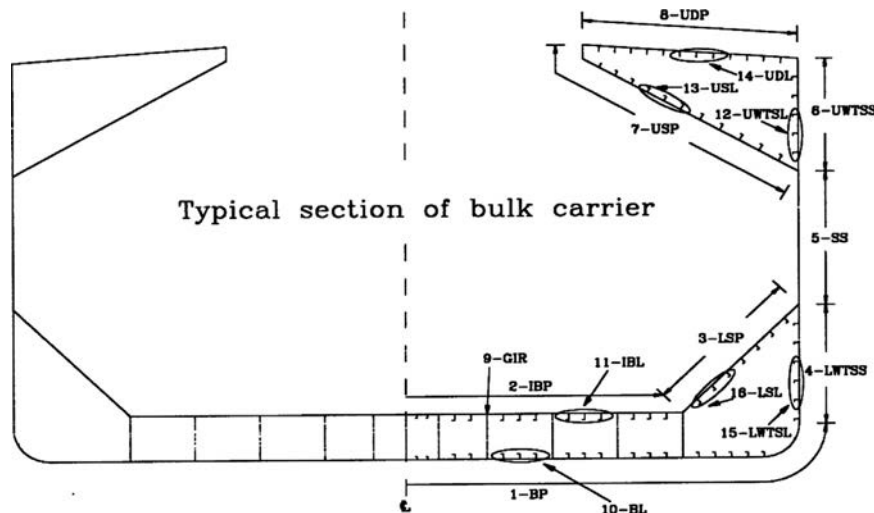


Fig. 1. Longitudinal primary members of bulk carrier [19].

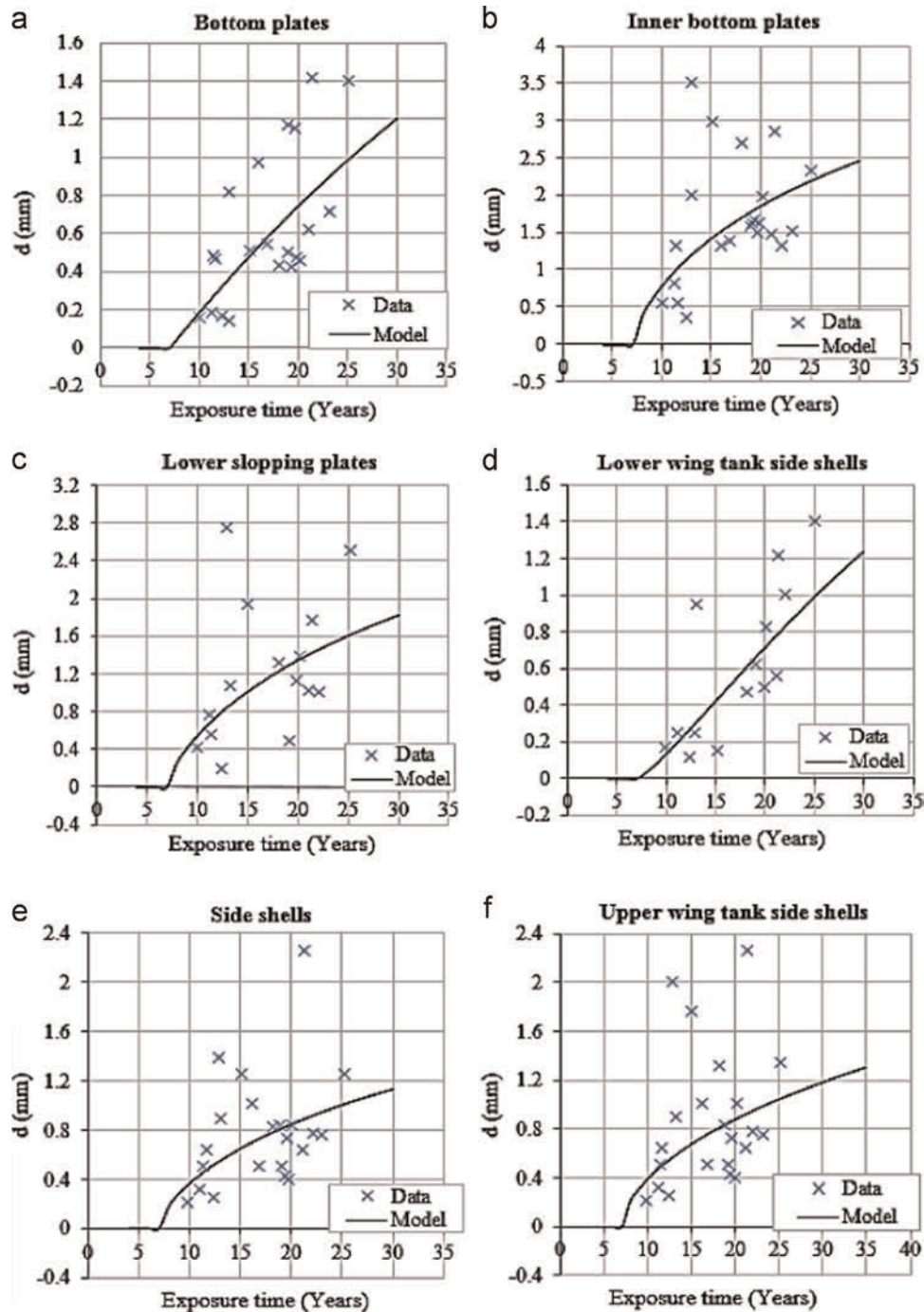


Fig. 2. Corrosion prediction model at different structural locations in a bulk carrier: (a) bottom plates (BP); (b) inner bottom plates (IBP); (c) lower slopping plates (LSP); (d) lower wing tank side shells (LWTSS); (e) side shells (SS); and (f) upper wing tank side shells (UWTSS).

years in service are equivalent to 0.8, 1.4, 1.85 and 2.2 mm. The diameter of the pits is determined according to the frequently observed damage extent, ranging from 20 mm to 70 mm. One-sided corrosion damage is applied on the structure by offsetting the mid-plane section of the corrosion areas.

The material properties are equivalent to the ship grade high tensile steel ASTM A131. The length and thickness of the plate are determined according to the aspect ratio, α , of 1–4, and the plate slenderness ratio, β , of 1.5, 2.5, 3.5 and 4.5, which are typical values found around the mid-section of a bulk carrier [23]. Table 1 summarises the geometry and material properties utilised for the plates as well as the applied corrosion features.

Analysis is also conducted on a stiffened panel with four

longitudinal stiffeners as shown in Fig. 4 using the same material. Corrosion was applied on the plate area in the same manner as in Fig. 3. Angle type sections ISA 5030 6, ISA 7045 6 and ISA 10065 6 are used for the stiffeners with dimensions presented in Table 2. These give column slenderness ratio, λ , values of 0.55, 0.33 and 0.22 for $\alpha=3$, which are typically found in bulk carriers [23].

2.4. Nonlinear FEA verification

Verification of the nonlinear FEA is performed by replicating the work done by Paik et al. [14] and Kumar et al. [24]. The obtained stress–strain relationships for a number of DOPs are shown in Fig. 5, which correlates well with the published results given by

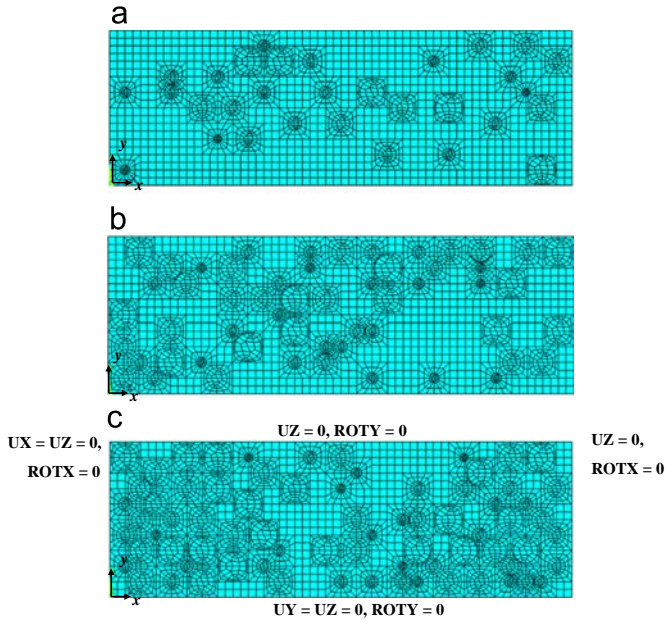


Fig. 3. Meshed plates for $\alpha=2$: (a) 10% DOP; (b) 20% DOP; (c) 30% DOP (simply supported boundary conditions: UX, UY, UZ: translation constraints in x-, y- and z-directions; ROTX, ROTY: rotation constraints about x- and y-axis).

Table 1
Material and geometric properties of plate models.

Properties	Value
b (mm)	400
a (mm)	400, 800, 1200 and 1600
t (mm)	11.04, 6.62, 4.73 and 3.68
E (GPa)	205.8
σ_y (MPa)	352.8
ν	0.3
E_t (GPa)	0
Initial imperfection	$w = 0.1\beta^2 t \sin(\frac{m\pi x}{a}) \sin(\frac{n\pi y}{b})$
Pit diameter (mm)	20–70
Pit shape	Circular
DOP (%)	10, 20 and 30

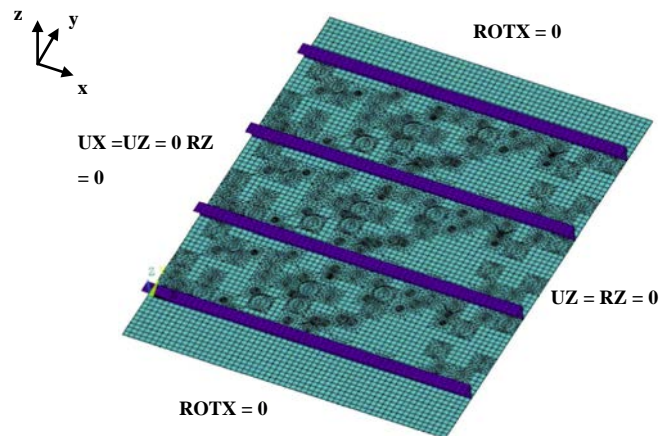


Fig. 4. Meshed stiffened panel (simply supported boundary conditions: UX, UY, UZ: translation constraints in x-, y- and z-directions; ROTX: rotation constraints about x-axis).

Paik et al. [14]. Small discrepancies may be associated with the differences in the modelling techniques. In the present study, the corrosion thickness is reduced by offsetting the reference plane (mid-plane) of the shell elements, while Paik et al. [14] assumed a

Table 2
Indian standard angle dimensions of stiffeners.

Indian standard angle type	Overall stiffener height (mm)	Flange breadth (mm)	Web and flange thickness (mm)
ISA5030 6	50	30	6
ISA7045 6	70	45	6
ISA10065 6	100	65	6
ISA12595 6	125	95	6

segmented plate thickness, setting the material properties throughout the corrosion depth to zero.

A stiffened panel with a circular cut-out developed by Kumar et al. [24] is replicated for verifying the stiffened panel model. Although the cut-out may not represent corrosion damage, the purpose is to verify the modelling of the plate-stiffener geometry. The normalised axial load was plotted against the plate slenderness ratio, β , for a range of column slenderness ratios, $\sigma\lambda$, as shown in Fig. 6. Again, the replicated models show a good agreement with the published ones. The small differences in the ultimate strength values could possibly be due to different material properties which are not clearly specified in the report [24]. These include the shape of the initial imperfection and the material model used. Thus, the verification has presented a reasonably good degree of confidence in the nonlinear FEA structural modelling technique.

3. FEA analysis of corroded structures

To investigate the manner in which corrosion affects steel structures a parametric study has been performed on a plate and a stiffened panel. The load and deflection values for each substep were extracted from ANSYS and plotted as normalised stress, σ_n , and strain, ϵ_n

$$\sigma_n = \frac{P}{\sigma_y b t}; \quad (2)$$

$$\epsilon_n = \frac{X}{(\sigma_y/E)a}; \quad (3)$$

where σ_y is the yield strength of the material, E is the Young's modulus, P is the external load, X is the displacement in the loading (x-) direction, t is the plate thickness and a and b are length and the width of the plate, respectively.

3.1. Parametric analysis of plate models

A plate model has been analysed first to determine the reduction in the ultimate strength capacity over time and investigate the effects of corrosion severity, aspect ratio and slenderness ratio.

3.1.1. Ultimate strength reduction over time

The ultimate strength reduction for a steel plate is assessed at different locations throughout the lifespan of a ship for $\beta=2.5$, $\alpha=3$ and 20% DOP. The ultimate strength (US) reduction is calculated using Eq. (4)

$$\text{US reduction (\%)} = \frac{\sigma_n(\text{Intact}) - \sigma_n(\text{corroded})}{\sigma_n(\text{Intact})} \times 100 \quad (4)$$

where $\sigma_n(\text{intact})$ and $\sigma_n(\text{corroded})$ are the normalised ultimate strength values at intact and corroded conditions, respectively. Fig. 7 shows as expected, the strength reduction increases in an approximately linear manner with increased exposure time in general. The IBP experiences the greatest reduction in ultimate

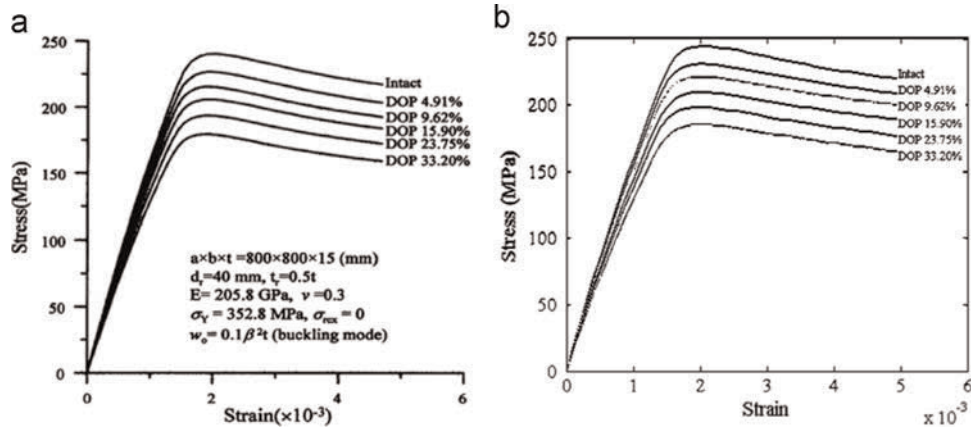


Fig. 5. Average axial compressive stress–strain curves for various DOPs with pit depth equals to half of the original plate thickness: (a) Paik et al.'s model [14] and (b) replicated model.

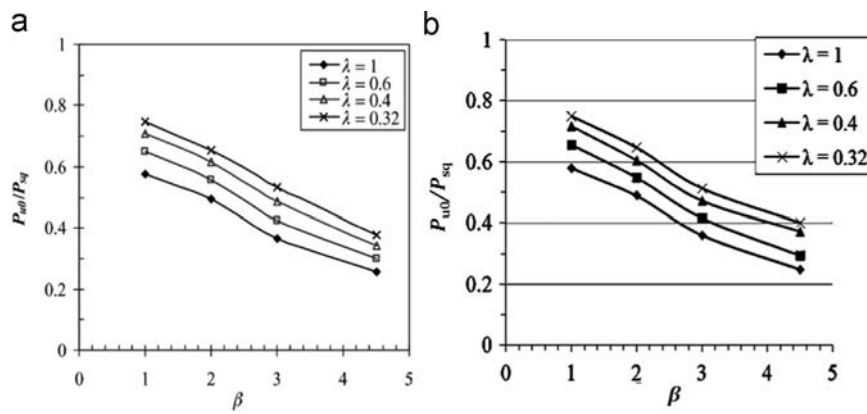


Fig. 6. Effect of column ratio and slenderness ratio on normalised axial load: (a) Suneel Kumar et al.'s model [24]; (b) replicated model.

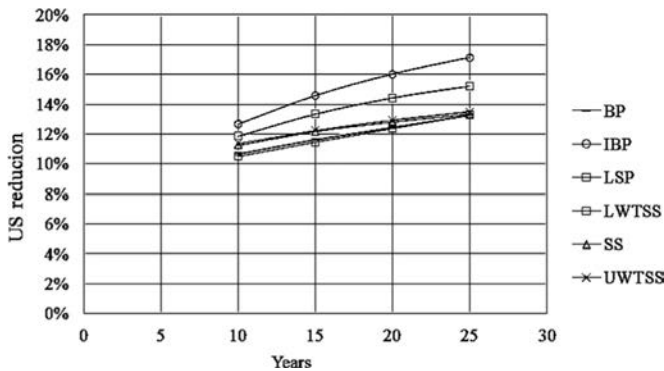


Fig. 7. Ultimate strength (US) reduction at different service life for plates at different locations of a bulk carrier.

strength with time, up to approximately 17% at 25 years in service. Although the initial strength reductions for the BP and LWTSS are relatively small, they become comparable with the SS and UWTSS conditions after 25 years exposure.

3.1.2. Effect of corrosion severity

To examine the corrosion severity effect, Fig. 8 shows the ultimate strength reduction of plate ($\alpha=3$) plotted against the corrosion-induced volume loss. Results show that for nearly all the plate slenderness ratios ($\beta=1.5, 2.5, 3.5$ and 4.5), the strength reduction is higher for larger corrosion area (DOP) and shallower pit for the same volume loss. The maximum drop in ultimate strength value is around 45.2% at a volume reduction of 18% for a slender plate, $\beta=4.5$. Fig. 9 shows the normalised stress–strain

curves for the IBP plates with $\beta=1.5$ and $\beta=3.5$ respectively. For both sets of curves, an increase in DOP leads to a greater strength reduction for every pit depth. For more stocky plates, $\beta=1.5$, the trend of the stress–strain plot is closer to that of an intact/virgin plate. The results for plate with $\beta=3.5$ show that the shape of the stress–strain curve varies significantly with DOP values, mainly in the post-collapse region.

3.1.3. Effect of aspect ratio α

The aspect ratio α is varied from 1 to 4 for three slenderness ratios ($\beta=1.5, 2.5$ and 4.5) for plates with 20% DOP and 2.2 mm pit depth. The results are plotted in Fig. 10. It can be observed that the ultimate strength of the plates varies with aspect ratio, especially for $\beta=1.5$. In general the results for $\alpha=2$ and 3 remain roughly half way between $\alpha=1$ and 4. However, for the $\beta=4.5$ case the final failure strength is similar for all α values. Therefore, as slenderness ratio increases, the effect of the aspect ratio gradually becomes insignificant. Similar results are also observed by Benson et al. [25] from an intact aluminium plate.

3.1.4. Effect of plate slenderness ratio β

As depicted in Fig. 11 the ultimate strength value gradually decreases with increasing plate slenderness ratio due to the plate thickness reduction. The transition from the onset of loading to the ultimate strength is longer for the most slender plate, implying a higher ultimate strain value. The post-collapse region behaviour becomes less stable when the slenderness ratio is beyond 3.

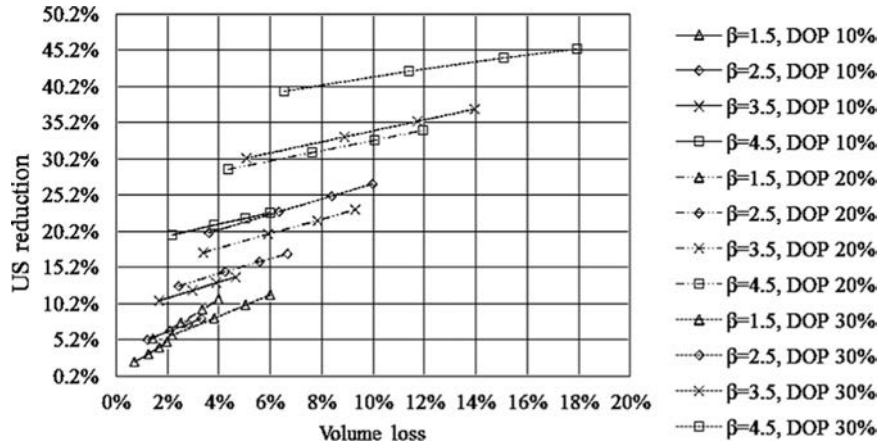


Fig. 8. Ultimate strength (US) reduction against corrosion-induced volume loss (%).

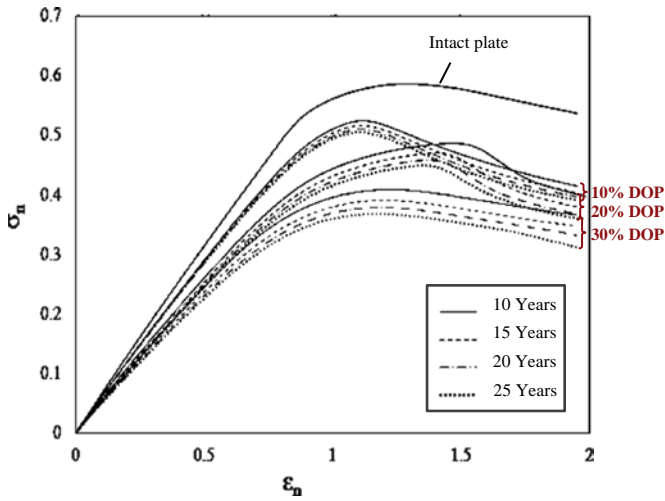


Fig. 9. Normalised stress–strain plots for IBP plates with $\alpha=3$ and $\beta=3.5$, varying the DOP and pit depth.

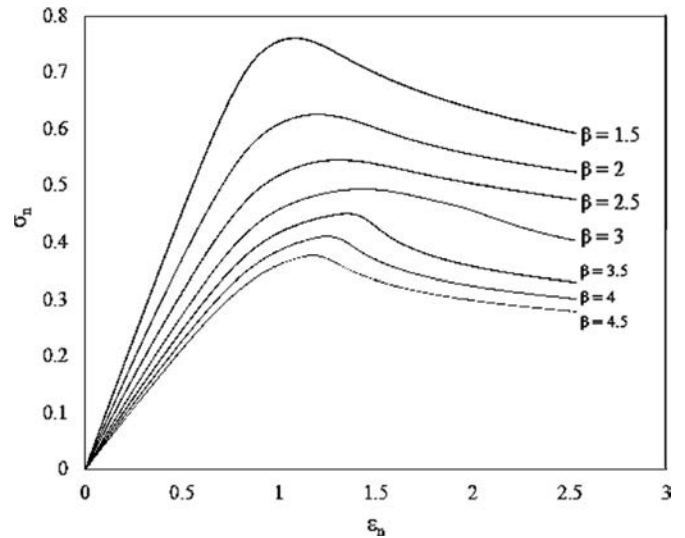


Fig. 11. Normalised stress–strain curves for plates at 20% DOP, pit depth=2.2 mm and $\alpha=3$.

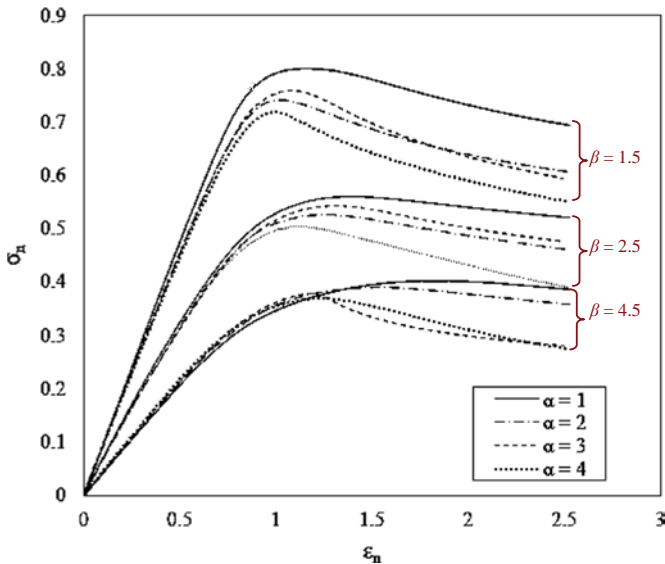


Fig. 10. Normalised stress–strain plots for plates at 20% DOP and pit depth=2.2 mm.

3.2. Parametric analysis of stiffened panel models

In comparison to the plate model, a stiffened panel model has been developed, focusing on the effects of corrosion severity,

aspect ratio, plate slenderness ratio and column slenderness ratio on the structural strength.

3.2.1. Effect of corrosion severity

A study on the effect of corrosion severity is undertaken varying the DOP and pit depth. It is interesting to see that for the same DOP, the ultimate strength reduction caused by increasing pit depth is more significant for panels consisting of plate elements with lower slenderness ratio, as shown in Fig. 12. This suggests that as the plates become more slender a larger percentage of the load is carried by the stiffeners and hence the effect of pitting corrosion would have less effect on the overall strength of the panel.

3.2.2. Effect of aspect ratio α

The aspect ratio is varied between 1 and 4 for three slenderness ratios ($\beta=1.5, 2.5$ and 4.5). The corrosion area and pit depth are kept constant (20% DOP and 2.2 mm, respectively, where the pit depth is equivalent to 25 years exposure for the IBP panels). For each of these cases the behaviour is more sensitive to the change in both aspect and slenderness ratio. From Fig. 13 it can be seen that there is a significant decrease in the ultimate strength for $\alpha=4$, associated with an interframe failure mode. Corrosion location also has an influence on the stress–strain behaviour. However, due to the random nature of the pit distribution and the

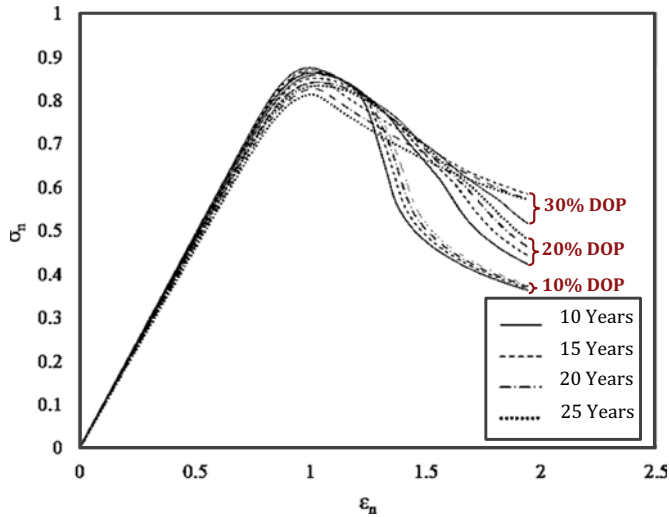


Fig. 12. Normalised stress–strain plots for $\alpha=3$, $\beta=1.5$ and $\lambda=0.33$ varying the DOP and pit depth.

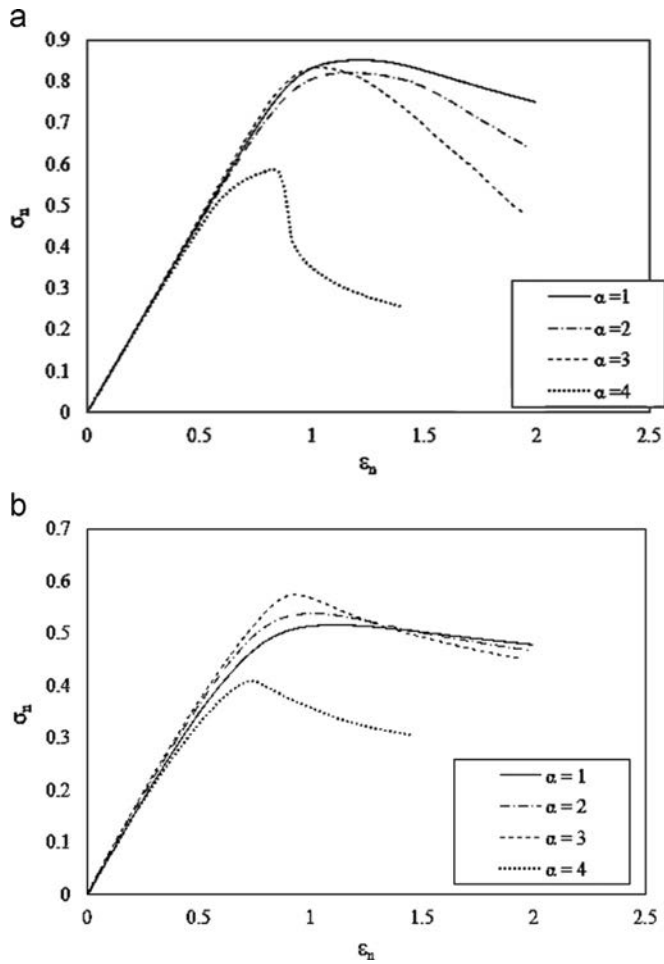


Fig. 13. Normalised stress–strain plot for stiffened panel 20% DOP and 2.2 mm pit depth: (a) $\beta=1.5$ and (b) $\beta=4.5$.

difference in the initial imperfections, it is noticed that the maximum displacement location does not always reflect the location where there is a high level of pitting.

3.2.3. Effect of plate slenderness ratio β

The plate slenderness ratio is varied between 1.5 and 4.5 to analyse its effect on the ultimate strength of a corroded stiffened

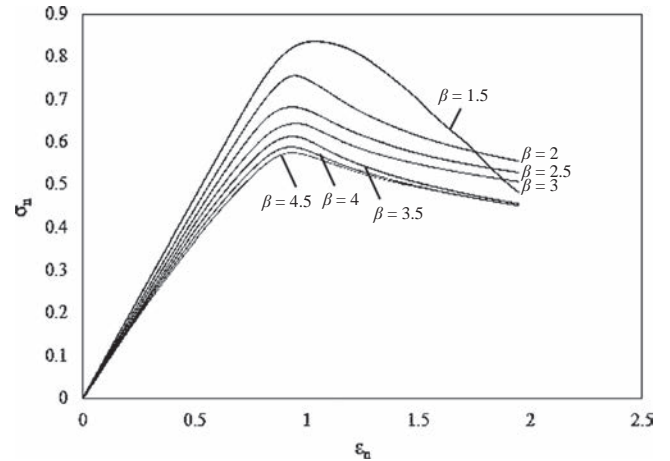


Fig. 14. Normalised stress–strain curves of stiffened panels at DOP=20%, pit depth=2.2 mm, $\alpha=3$ and $\lambda=0.3$.

panel. The stress–strain results are plotted in Fig. 14. Similar to the plate models (Fig. 11), the strength reduces with increasing plate slenderness ratio. The general trend of the plots is similar, suggesting a similar failure mode and behaviour of the structures. However, for the stockiest stiffened panel ($\beta=1.5$), the behaviour of the panel in the post-collapse region is slightly different: peaking at a higher value and reducing to below the other panels.

3.2.4. Effect of column slenderness ratio λ

The ultimate strength of the stiffened panel is found to decrease with increased column slenderness ratio (increased web height and decreased flange width). Fig. 15 shows the manner in which the strength reduction for an increase in λ is larger, independent of the β value. The similar trend of the curves suggests that the failure mode is similar for each condition.

4. Discussion

4.1. Plate models

The ultimate strength reduction assessment with time is based on the corrosion prediction model and the survey data (Fig. 2). The reduction values for all locations are approximately linearly increased as aging (Fig. 7). The LSP and the IBP experienced the largest decrease in ultimate strength as these two locations are

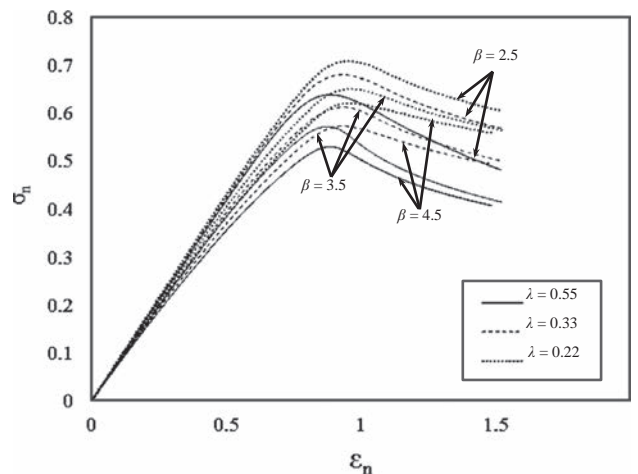


Fig. 15. Normalised stress–strain curves of stiffened panels at DOP=20%, pit depth=2.2 mm and $\alpha=3$.

directly in contact with both ballast water and/or cargoes (Fig. 1) which could be highly corrosive [4]. Moreover, direct contact of the cargo such as iron ore on the structural plates may cause the protective coating/oxide layer break-off and expose the underlying metallic surface. Although the locations of LSP and IBP are close to each other, the difference in the structural orientation could lead to differences in the corrosion rate and hence the strength capacity, with the latter being exceptionally vulnerable due to the water/sediment accumulation on the structural surface. For the locations of BP and LWTSS, although coating/anti-fouling system is periodically renewed, the result of the seawater velocity may accelerate the corrosion process and lead to a greater strength loss as the service life increases. For the same corrosion-induced volume loss, the greater strength reduction associated with high DOP values (Fig. 8) is found to be caused by the pitting location variations. As the DOP increases, the pitting damage is more located along the plate edges (Fig. 3). This significantly affects the stress redistribution at the onset of yielding, and hence a much lower ultimate strength. The percentage of the volume loss is smaller for plates with a lower slenderness ratio, resulting in less effect on the stress–strain relationships (Fig. 9(a)). The stress concentration initiates around the corrosion pits which are situated close to the unloaded edges. This characteristic is also observed in previous research in Wang et al. [16].

Regarding the aspect ratio effects, the failure mode and the ultimate strength is found to be related to the initial deflection, which varies for different aspect ratios. Higher aspect ratios may lead to a reduced plate thickness for a fixed β , and hence a lower ultimate strength (Fig. 10). However, as the slenderness ratio increases, the influence of the aspect ratio becomes negligible.

For plates with higher slenderness ratios, the larger strain value obtained at the collapse point (Fig. 11) is found to be the result of the transition from the shape of the applied initial deflection to the shape of the actual buckling mode. For example in Fig. 16, the buckling mode for $\beta=1.5$ is similar to the initial imperfection shape, while for less stocky plates, higher β , at the collapse point the maximum deflection shifts towards one of the loaded edges, resulting in much more localised plasticity and a lower ultimate strength. As indicated in Wang et al. [16], corrosion at the edges has a more detrimental effect on lowering the strength capacity, which explains the much reduced strength value for plates with high β .

4.2. Stiffened panel models versus plate models

For stiffened panels, when the plate elements are of high slenderness ratio, the stiffeners play a more significant role in taking the load and redistributing the stress, which results in a smaller effect of corrosion severity compared to the plate models, as for the case of $\beta=4.5$ in Figs. 9(b) and 12(b). However, the ultimate strength of a stiffened panel can be severely affected when corrosion occurs on the stiffener.

For both plate and stiffened panel models it is evident that an increase in the plate aspect ratio does not always result in a decrease in ultimate strength (Figs. 10 and 13). The much reduced ultimate strength of the panel at $\alpha=4$ in Fig. 13 is mainly linked to the failure mode. Analysing the von Mises stress distribution it is found that in nearly all cases, yielding initiates at the plate-stiffener intersections at the edges and in some cases also at around mid-span. For $\beta=1.5$ and $\alpha=1, 2$ and 3 the failure mode is due to yielding along the stiffener (Fig. 17(a)). However, for $\alpha=4$, yielding occurs at the plate-stiffener intersection at the edges as shown in Fig. 17(b). From Fig. 13(b) it can be seen that the panel with $\alpha=3$ has the highest ultimate strength value. Meanwhile, a higher column slenderness ratio leads to a lower ultimate strength (Fig. 15). As the external load increases, it is found that for $\alpha=3$

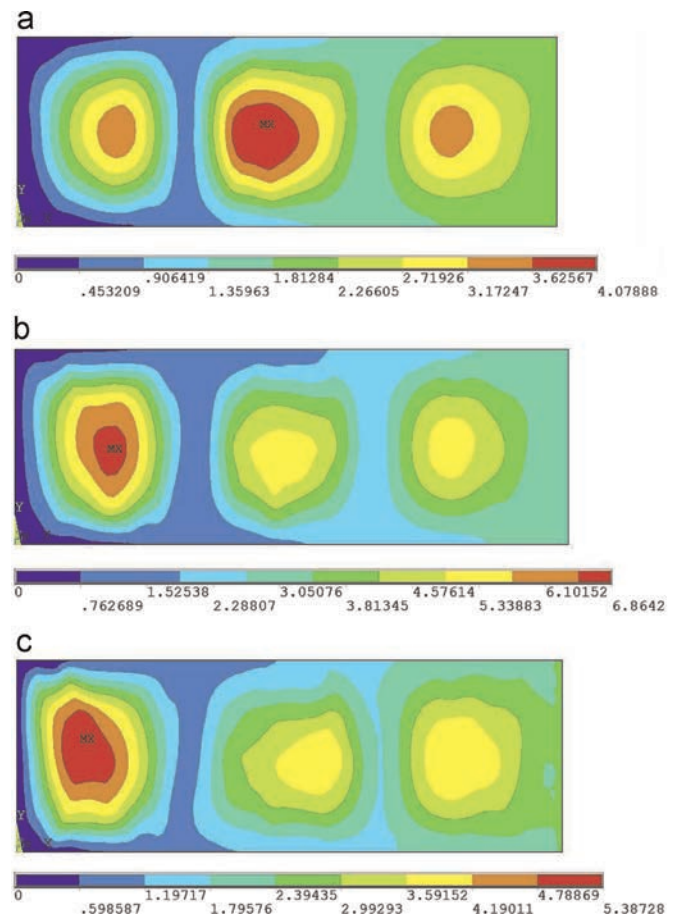


Fig. 16. Out-of-plane displacement (mm) plots at ultimate strength stage for $\alpha=3$, 20% DOP, pit depth=2.2 mm: (a) $\beta=1.5$; (b) $\beta=3$; and (c) $\beta=4.5$.

and $\lambda=0.33$ the stress concentration is along the longitudinal stiffener until the ultimate strength point, as depicted in Fig. 17 (a) and (c), indicating that the ultimate strength state is attended with an extensive development of yielding on the stiffener. Conversely, yielding for $\alpha=4$ and $\lambda=0.44$ occurs at the edges as shown in Fig. 17(b) and (d), meaning that the stiffener makes less contribution in carrying extra load.

Generally, in both cases for larger β value, the residual strength is lower as depicted in Figs. 11 and 14. However, the overall reduction in strength for the stiffened panel is smaller. This is because as β increases, higher loads would be carried by the stiffeners which would also lead to a less significant effect from corrosion. Moreover, the out-of-plane displacement of stiffened panel models at the ultimate strength for $\beta=1.5$ shows an overall increase with the maximum amplitude being around mid-span while for $\beta=4.5$, the high deformation occurs mainly at local plating area. As a result the former would lead to an overall collapse failure, while the more slender panel would fail due to interframe collapse. Stress distribution similar to Fig. 17(c) is observed for panels which plate slenderness ratio lies between 2 and 4.5.

5. Conclusions

Corrosion can have a detrimental effect on the strength capacity of a steel structure. To predict the strength during the life of the structure corrosion must be taken into account. Many studies focus on the effects of corrosion on unstiffened plate models. The nonlinear FEA is used here to investigate the effect of random

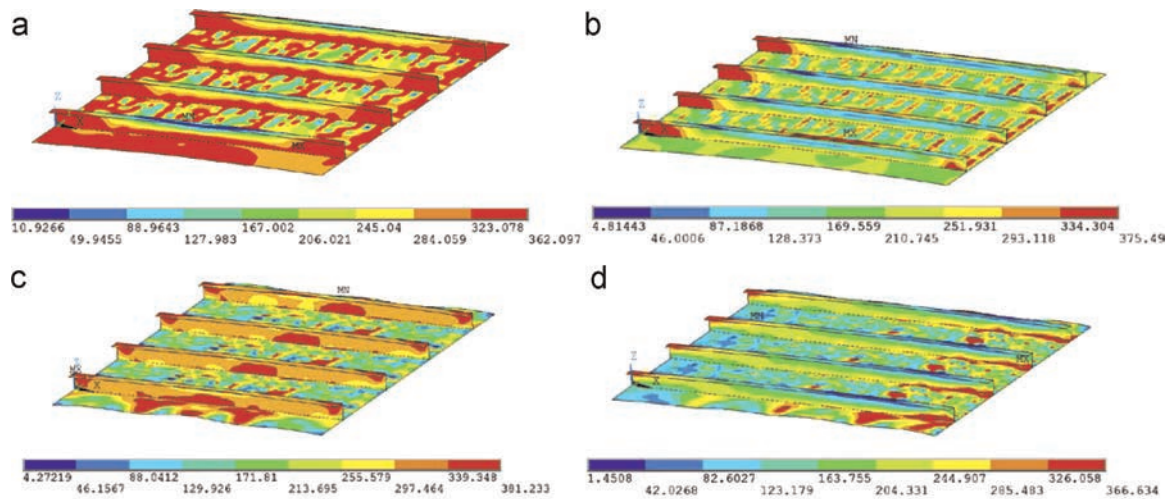


Fig. 17. Von Mises stress (MPa) contour plots for stiffened panels: (a) $\alpha=3$, $\beta=1.5$ and $\lambda=0.33$; (b) $\alpha=4$, $\beta=1.5$ and $\lambda=0.44$; (c) $\alpha=3$, $\beta=4.5$ and $\lambda=0.33$; and (d) $\alpha=4$, $\beta=4.5$ and $\lambda=0.44$.

pitting corrosion on the strength capacity of steel plates and compares these results to stiffened panels. In general, it can be concluded that for most cases the behaviour of plates and stiffened panels are consistent as parameters vary, however, there are exceptions. Rectification of the boundary conditions for plate could possibly lead to better consistency but appropriate selection of the boundary conditions for plate to try to replicate the effect of the stiffeners is considered to be difficult. Overall, the structural element selection, i.e., size, form and location, was shown to influence the accuracy of the estimated corrosion damage showing some differences in failure mode and in some parametric trends. The key findings are summarised as follows:

- (1) Ultimate strength reduces with increasing column slenderness ratio for the studied stiffened panels, of which the typical failure mode is beam-column type;
- (2) for the plate model a volume loss of around 18% can lead to up to 45% reduction in the ultimate strength;
- (3) a larger slenderness ratio is associated with a lower ultimate strength for both structures. However, the overall strength reduction for stiffened panels is smaller than for plates;
- (4) the mechanical behaviour of a corroded structural member is largely dependant on the corrosion location, severity and the initial deflection shape.
- (5) for both plates and stiffened panels subjected to pitting corrosion, an increase in the plate aspect ratio does not always reduce the ultimate strength. A significant drop in ultimate strength is evident for the stiffened panels with an aspect ratio of 4. However, this behaviour was not seen for the plate models.

Further studies are needed to effectively identify the distribution of corrosion damage for different structural locations with time. Full scale testing is also essential to understand the physical responses to various corrosion mechanisms, as well as to validate the numerical analysis.

Acknowledgement

The authors gratefully acknowledge the funding by the University of Southampton and Lloyd's Register Foundation University Technology Centre (LRF UTC). The research is also partially funded by the "MASTER it!" Scholarship Scheme. The scholarship is part-financed by the European Union – European Social Fund.

References

- [1] ISSC, Report of Specialist Committee III.1 Ultimate Strength, in: Proceedings of the 17th International Ship and Offshore Structures Congress, Seoul, Korea, 2009, pp. 375–474.
- [2] J.K. Paik, A.K. Thayamballi, *Ultimate Limit State Design of Steel-Plated Structures*, John Wiley & Sons, England, 2003.
- [3] R. a. E. o. A. W. P. Centre of Documentation, Prestige, Cedre, [Online]. Available: (<http://www.cedre.fr/en/spill/prestige/prestige.php>) (accessed 28.04.14).
- [4] Y. Wang, J.A. Wharton, R.A. Shenoi, Ultimate strength analysis of aged steel-plated structures exposed to marine corrosion damage: a review, *Corros. Sci.* 86 (2014) 42–60.
- [5] R.E. Melchers, T. Wells, Models for the anaerobic phases of marine immersion corrosion, *Corros. Sci.* 48 (2006) 1791–1811.
- [6] J.K. Paik, D.K. Kim, Advanced method for the development of an empirical model to predict time-dependent corrosion wastage, *Corros. Sci.* 63 (2012) 51–58.
- [7] M. Hairil Mohd, D.K. Kim, D.W. Kim, J.K. Paik, A time-variant corrosion wastage model for subsea gas pipelines, *Ships Offshore Struct.* 9 (2014) 161–176.
- [8] M. Hairil Mohd, J.K. Paik, Investigation of the corrosion progress characteristics of offshore subsea oil well tubes, *Corros. Sci.* 67 (2013) 130–141.
- [9] S. Qin, W. Cui, Effect of corrosion models on the time-dependent reliability of steel plated elements, *Mar. Struct.* 16 (2003) 15–34.
- [10] X. Jiang, C. Guedes Soares, Assessment of the uncertainty in corrosion models for ship steels, in: Proceedings of the 27th International Conference on Off-shore Mechanics and Arctic Engineering (OMAE 2008). ASME, Estoril, Portugal, 2008.
- [11] S. Saad-Eldeen, Y. Garbatov, C. Guedes Soares, Effect of corrosion severity on the ultimate strength of a steel box girder, *Eng. Struct.* 49 (2013) 560–571.
- [12] J.E. Silva, Y. Garbatov, C. Guedes Soares, Reliability assessment of a steel plate subjected to distributed and localized corrosion wastage, *Eng. Struct.* 59 (2014) (23–20).
- [13] J.E. Silva, Y. Garbatov, C. Guedes Soares, Ultimate strength assessment of rectangular steel plates subjected to a random localised corrosion degradation, *Eng. Struct.* 52 (2013) 295–305.
- [14] J.K. Paik, J.M. Lee, M.J. Ko, Ultimate compressive strength of plate elements with pit corrosion wastage, *Proc. Inst. Mech. Eng. Part M: J. Eng. Marit. Environ.* 217 (2003) 185–200.
- [15] Y. Huang, Y. Zhang, G. Liu, Q. Zhang, Ultimate strength assessment of hull structural plate with pitting corrosion damage under biaxial compression, *Ocean Eng.* 37 (2010) 1503–1512.
- [16] Y. Wang, J.A. Wharton, R.A. Shenoi, Influence of localised pit distribution and bench-shape pits on the ultimate compressive strength of steel plating for shipping, *Corrosion* 70 (2014) 915–927.
- [17] Y. Wang, J.A. Wharton, R.A. Shenoi, Ultimate strength assessment of steel stiffened plate structures with grooving corrosion damage, *Eng. Struct.* 94 (2015) 29–42.
- [18] J.K. Paik, J.K. Seo, Nonlinear finite element method models for ultimate strength analysis of steel stiffened-plate structures under combined biaxial compression and lateral pressure actions-Part I: Plate elements, *Thin-Walled Struct.* 47 (2009) 1008–1017.
- [19] J.K. Paik, S.K. Kim, S.K. Lee, Probabilistic corrosion rate estimation model for longitudinal strength members of bulk carriers, *Ocean Eng.* 25 (1998) 837–860.
- [20] ABS, The inspection, Maintenance and Application of Marine Coating Systems, 2007. [Online]. Available: (http://www.eagle.org/eagleExternalPortalWEB/ShowProperty/BEA%20Repository/Rules&Guides/Current/49_In)

- [spMaint&ApplofMarineCoatingSystems/Pub49_CoatingsNov07](#)). (accessed 12.08.14).
- [21] ABS, Guide for hull thickness measurement, in: Rules for Survey after Construction. American Bureau of Shipping Houston, USA, 2009.
- [22] J.C. Daidola, J. Parente, I.R. Orisamolu, K. Ma, Residual strength assessment of pitted plate panels, in: Ship Structure Committee Report SSC-394, 1997.
- [23] S. Zhang, I. Khan, Buckling and ultimate capability of plates and stiffened panels in axial compression, *Mar. Struct.* 22 (2009) 791–808.
- [24] M. Suneel Kumar, P. Alagusundaramoorthy, R. Sundaravadivelu, Interaction curves for stiffened panel with circular opening under axial and lateral loads, *Ships Offshore Struct.* 4 (2009) 133–143.
- [25] S. Benson, J. Downes, R.S. Dow, Ultimate strength characteristics of aluminium plates for high-speed vessels, *Ships Offshore Struct.* 6 (2011) 67–80.